

TYPE Ia SUPERNOVAE: INFLUENCE OF THE INITIAL COMPOSITION ON THE  
NUCLEOSYNTHESIS, LIGHT CURVES, AND SPECTRA AND CONSEQUENCES  
FOR THE DETERMINATION OF  $\Omega_M$  AND  $\Lambda$

P. HÖFLICH,<sup>1,2,3</sup> J. C. WHEELER,<sup>1,3</sup> AND F. K. THIELEMANN<sup>2,3</sup>

Received 1997 July 17; accepted 1997 October 13

ABSTRACT

The influence of the initial composition of the exploding white dwarf on the nucleosynthesis, light curves, and spectra of Type Ia supernovae has been studied in order to evaluate the size of evolutionary effects on cosmological timescales, how the effects can be recognized, and how one may be able to correct for them.

The calculations are based on a set of delayed detonation models that give a good account of the optical and infrared light curves and of the spectral evolution. The explosions and light curves are calculated using a one-dimensional Lagrangian radiation-hydro code including a nuclear network. Spectra are computed for various epochs using the structure resulting from the light-curve code. Our non-LTE code solves the relativistic radiation transport equations in the comoving frame consistently with the statistical equations and ionization due to  $\gamma$ -radiation for the most important elements (C, O, Ne, Na, Mg, Si, S, Ca, Fe, Co, Ni). About  $10^6$  additional lines are included assuming LTE-level populations and an equivalent–two-level approach for the source functions.

Changing the initial metallicity  $Z$  from Population I to Population II alters the isotopic composition of the outer layers of the ejecta that have undergone explosive O burning. Especially important is the increase of the  $^{54}\text{Fe}$  production with metallicity. The influence on the resulting rest-frame visual and blue light curves is found to be small. Detailed analysis of spectral evolution should permit a determination of the progenitor metallicity.

Mixing  $^{56}\text{Ni}$  into the outer layers during the explosion can produce effects similar to an increased initial metallicity. Mixing can be distinguished from metallicity effects by means of the strong cobalt and nickel lines, by a change of the calcium lines in the optical and IR spectra and, in principle, by  $\gamma$ -ray observations.

As the C/O ratio of the white dwarf is decreased, the explosion energy and the  $^{56}\text{Ni}$  production are reduced, and the Si-rich layers are more confined in velocity space. A reduction of the C/O ratio by about 60% gives slower rise times by about three days, an increased luminosity at maximum light, a somewhat faster postmaximum decline, and a larger ratio between maximum light and  $^{56}\text{Ni}$  tail. A reduction of the C/O ratio has an effect on the colors, light-curve shapes and element distribution similar to a reduction in the deflagration to detonation transition density. However, for the same light-curve shape, the absolute brightness is larger for smaller C/O ratios. An independent determination of the initial C/O ratio and the transition density is possible for local supernovae if detailed analyses of both the spectra and light curves are performed simultaneously.

Because the spectra are shifted into different color bands at different redshifts, the effect of metallicity  $Z$  on a given observed color is a strong function of redshift. A change of  $Z$  by a factor of 3 or of the C/O ratio by 33% alters the peak magnitudes in the optical wavelength range by up to  $\approx 0.3$  mag for  $z \geq 0.2$ . These variations are comparable to the effect of changes of  $\Omega_M$  and  $\Lambda$  at redshifts of 0.5–1.0. The systematic effects due to changes in composition are expected to remain small up to about  $z \approx 0.5$  for  $R - V$  and up to  $z \approx 0.7$  for  $R - I$ .

We discuss how evolution in the progenitor population can be recognized and taken into account. With proper account of evolutionary corrections, supernovae will provide a valuable tool to determine the cosmological parameters of the universe, and they will provide new insight into its chemical evolution.

*Subject headings:* cosmology: theory — hydrodynamics — nuclear reactions, nucleosynthesis, abundances — stars: evolution — stars: interiors — supernovae: general

1. INTRODUCTION

Type Ia supernovae (SNe Ia) may reach the same brightness as the entire parent galaxy. In principle, this allows for the measurements of extragalactic distances and cosmological parameters such as the Hubble constant  $H_0$ ,  $\Omega_M$ ,  $\Omega_\Lambda$ ,

and the related deceleration parameter  $q_0$ . It is now widely accepted that SNe Ia are not a strictly homogeneous class of objects with similar brightness (e.g., Barbon, Ciatti, & Rosino 1973; Barbon et al. 1990; Pskovskii 1970, 1977; Branch 1981; Phillips et al. 1987; Filippenko et al. 1992a; 1992b; Leibundgut et al. 1991; Hamuy et al. 1996). For nearby supernovae ( $z \leq 0.1$ ), different schemes have been developed and tested to cope with the problems of deducing (1) the intrinsic brightness based on theoretical models or observed correlations between spectra or light curves and

<sup>1</sup> Department of Astronomy, University of Texas, Austin, TX 78712.

<sup>2</sup> Department of Physics and Astronomy, University of Basel, CH-4056 Basel, Switzerland.

<sup>3</sup> Institute for Theoretical Physics, University of California, Santa Barbara, CA 93186-4030.

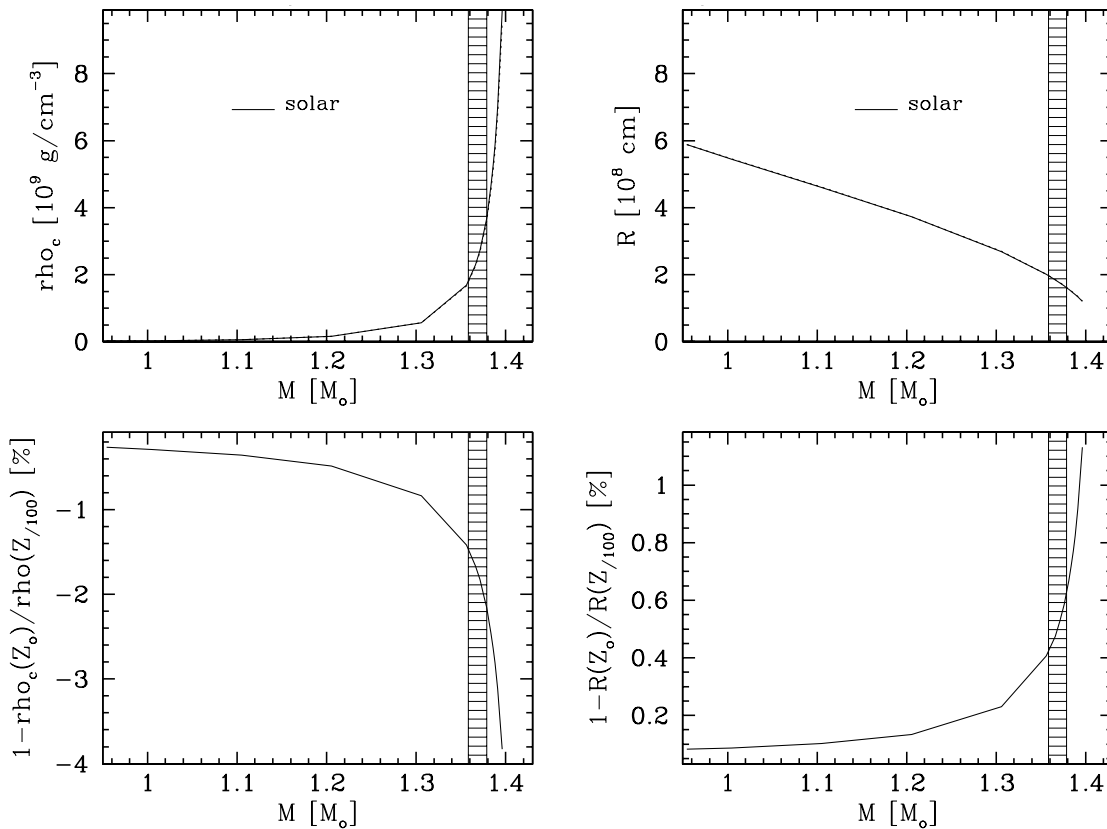


FIG. 1.—Influence of the metallicity on the central density  $\rho_c$  and radius  $R$  of a WD. The shaded band marks the region that allows for a successful reproduction of observed light curves and spectra for SNe Ia (Höflich & Khokhlov 1996). In the upper plots the  $M$ - $R$  relation and the  $\rho_c$ - $M$  relations are given for solar metallicities, and in the lower plots the difference (in %) for models with 1/100 of solar metallicity are given. On the scales of the upper plots, the curves corresponding to different metallicities would merge.

(2) the absolute brightness using primary distance indicators (e.g., Norgaard-Nielsen et al. 1989; Branch & Tammann 1992; Sandage & Tammann 1993; Müller & Höflich 1994; Hamuy et al. 1996; Riess, Kirshner, & Press 1995; Nugent et al. 1995; Höflich & Khokhlov 1996). These methods have been tested locally and provide consistent results. New telescopes and observational programs put SNe Ia at large redshifts well within reach and justify optimism for the discovery of a large number of distant SNe Ia. The Berkeley group has discovered more than 50 SNe Ia up to a redshift of 0.9 (Pennypacker et al. 1991; Perlmutter et al. 1997; C. Pennypacker 1997, private communication). The CfA/CTIO/ESO/MSSSO collaboration has found a similar number of supernovae (Leibundgut et al. 1995; Schmidt et al. 1996). Systematic errors due to evolutionary effects represent a concern for the use of SNe Ia to determine the shape of the universe (Höflich et al. 1997). This is especially true for statistical methods that are calibrated only on local SNe Ia. This paper represents a first attempt to characterize some of these evolutionary effects and points the way to elimination of associated systematic errors.

It is widely accepted that SNe Ia are thermonuclear explosions of carbon-oxygen white dwarfs (Hoyle & Fowler 1960; for discussions of various theoretical aspects see Woosley & Weaver 1986, 1994a; Wheeler & Harkness 1990; Canal 1994; Nomoto et al. 1995; Nomoto et al. 1997; Wheeler et al. 1995; Höflich & Khokhlov 1996). Three main scenarios can be distinguished:

A primary scenario consists of massive carbon-oxygen white dwarfs (WDs) with a mass close to the Chandrasek-

har mass that accrete through Roche lobe overflow from an evolved companion star (Nomoto & Sugimoto 1977; Nomoto 1982). In these accretion models, the explosion is triggered by compressional heating. From the theoretical standpoint, the key questions are how the flame ignites and how it propagates through the WD. Several models of SNe Ia within this general scenario have been proposed in the past, including detonations (Arnett 1969; Hansen & Wheeler 1969), deflagrations (Ivanova, Imshennik, & Chetkin 1974; Nomoto, Sugimoto, & Neo 1976), and delayed detonations, which assume that the flame starts as a deflagration and later turns into a detonation (Khokhlov 1991; Yamaoka et al. 1992; Woosley & Weaver 1994a). The latter scenario, the so-called delayed detonation and its variation, “pulsating delayed detonation,” seems to be the most promising one because, from the general properties and the individual light curves and spectra, it can account for the majority of SNe Ia events (e.g., Höflich & Khokhlov 1996; Höflich et al. 1997; Nomoto et al. 1997; Nugent et al. 1997 and references therein). In addition, with the discovery of the supersoft X-ray sources, potential progenitors have been found (van den Heuvel et al. 1992; Rappaport et al. 1994a, 1994b; DiStefano et al. 1997). We note that the classical “deflagration” model W7 has a similar structure to the “delayed detonation” models which have been successfully applied to reproduce light curves and spectra of normal bright SNe Ia (Harkness 1991).

The second scenario for progenitor models consists of two WDs in a close orbit that decays as a result of the emission of gravitational radiation. This, eventually, leads

to the merging of the two WDs. In an intermediate step, these models form a low-density WD surrounded by a CO envelope (Webbink 1984; Iben & Tutukov 1984; Paczyński 1985; Iben 1997).

A third class of models involves double detonation of a C-O WD triggered by detonation of a helium layer in low-mass WDs as explored by Nomoto (1980), Woosley, Weaver, & Taam (1980), and most recently by Woosley & Weaver (1994b); Livne & Arnett (1995) and Höflich & Khokhlov (1996). From light curves and spectra, this scenario can be excluded as accounting for the majority of SNe Ia events (Höflich et al. 1997; Nugent et al. 1997).

A separate but closely related uncertainty is the evolution of the progenitor systems (e.g., Hernanz et al. 1997). If the progenitor population undergoes a change with time, methods to determine  $\Omega_M$  and  $\Lambda$  (and hence  $q_0$ ) using only local calibrators could be systematically flawed.

Time evolution is expected to produce the following main effects: (1) A lower metallicity will decrease the timescale for stellar evolution of individual stars by about 20% from Population I to Population II stars (Schaller et al. 1992), and consequently alters the progenitor population that contributes to the SNe Ia rate at any given time. The stellar radius also shrinks. This will influence the statistics of systems with mass overflow. (2) Evolutionary effects of the stellar population will change the mass function present at the time corresponding to a given redshift. (3) The initial metallicity will determine the electron/nucleon fraction of the outer layers and thus affects the products of nuclear burning. (4) Systems with a shorter lifetime may dominate early on, and consequently the typical C/O ratio of the central region of the WD will be reduced. (5) The properties of the interstellar medium may change. (6) In principle, a change of the metallicity may alter the  $M$ - $R$  relation. Figure 1 shows that this issue is not a major concern.

In this paper we address the possible influence of evolutionary effects on light curves and spectra for the delayed detonation scenario. Because the time evolution of the composition is not well known, and because we have not considered the entire variety of possible models, the values given below *do not* provide a basis for quantitative corrections of existing observations. The goals are to get a first-order estimate of the size of the systematic effects, to demonstrate how evolutionary effects can be recognized in a real data sample, and to discover how one may be able to correct for them in the determination of cosmological parameters. In § 2 the numerical treatment is briefly described. In § 3 the influence of metallicity and the variation of the C/O ratio on the isotopic abundances, density, and velocity structure of the envelope are discussed. Light curves and maximum light spectra are presented. We discuss briefly how the effects of metallicity can be distinguished from mixing processes. In § 4 the influence of evolutionary effects on the use of SNe Ia to determine cosmological parameters is presented. Section 5 gives a discussion of our results and conclusions.

## 2. BRIEF DESCRIPTION OF THE NUMERICAL METHODS

### 2.1. Hydrodynamics

The explosions are calculated using a one-dimensional radiation-hydro code, including nuclear networks (Höflich & Khokhlov 1996). This code solves the hydrodynamical equations explicitly by the piecewise parabolic method

(Colella & Woodward 1984) and includes the solution of the radiation transport implicitly via momentum equations, expansion opacities, and a detailed equation of state (Höflich, Müller, & Khokhlov 1993). About 500 depth points are used. Radiation transport has been included to provide a smoother transition from the hydrodynamical explosion to the phase of free expansion. We omit  $\gamma$ -ray transport during the hydrodynamical phase because of the high optical depth of the inner layers. Nuclear burning is taken into account using our network, which has been tested in many explosive environments (see, e.g., Thielemann, Nomoto, & Hashimoto 1996 and references therein). During the hydrodynamical calculations, an  $\alpha$ -network of 14 isotopes is included to describe the energy release. The final chemical structure is calculated by postprocessing the hydrodynamical model using a network of 216 nuclei. The accuracy of the energy release in the reduced network has been found to be about 1%–3%.

### 2.2. Light Curves

Based on the explosion models, the subsequent expansion and bolometric as well as monochromatic light curves are calculated using a scheme recently developed, tested, and widely applied to SNe Ia (e.g., Höflich et al. 1993, 1997 and references therein). The code used in this phase is similar to that described above, but nuclear burning is neglected and  $\gamma$ -ray transport is included via a Monte Carlo scheme (Höflich, Müller, & Khokhlov 1992). In order to allow for a more consistent treatment of scattering, we solve both the (two lowest) time-dependent radiation momentum equations for the radiation energy and the radiation flux, and a total energy equation. At each time step we then use  $T(r)$  to determine the Eddington factors and mean opacities by solving the frequency-dependent radiation transport equation in the comoving frame (see next section) in about 100 frequency bands (see below) and integrate to obtain the frequency-averaged Eddington factors. We use the latter to iterate the solution with the frequency-integrated energy and flux equations. The frequency-averaged opacities, i.e., Planck, Rosseland, and flux means, have been calculated under the assumption of local thermodynamic equilibrium. This is a reasonable approximation for the light curve, since diffusion timescales are always governed by layers of large optical depths. Note that the comparison of  $L(r)$  between the frequency-independent solution and the frequency-dependent solution provides a critical test for the consistency of the approximations used in the radiation-hydro code.

Both the monochromatic and the mean opacities are calculated using the Sobolev approximation (Sobolev 1957) to calculate the absorption probability within a shell, and to include line blanketing. The approach is similar to that of Karp et al. (1977) but is generalized for the comoving frame, and the integration boundaries are adjusted to a radial grid (Höflich 1990). The scattering, photon redistribution, and thermalization terms used in the light-curve opacity calculation are calibrated with non-LTE (NLTE) calculations using the formalism of the equivalent–two-level approach (Höflich 1995).

To calculate the monochromatic light curves, we use the  $T(r)$ , with the time dependence of the structure given by the frequency-integrated solution of the momentum equations, to solve the frequency-dependent transfer equations in LTE every 0.2–0.5 days, and to get  $L_v$  in the observer's frame.

The broadband light curves are determined by convolution of  $L_\nu$  with the filter functions. We use a few hundred frequency bands with the scheme described in the following subsection. Note that a proper treatment of the frequency derivatives in the comoving frame equations requires the use of about 5–10 times more frequencies than frequency bands. To test the consistency between the frequency-dependent and frequency-independent calculations we also integrate the  $L_\nu$  and check to see how close the resulting  $L$  is to that from the solution of the frequency-integrated moment equations. The solutions are consistent within 10% as shown in Figure 2 (see also Khokhlov, Müller, & Höflich 1993). Monochromatic colors from our light-curve code have been compared to colors calculated by our detailed NLTE spectral code (Höflich 1995). Based on this comparison, the solutions for the Type Ia models are good to a few percent near maximum light and deteriorate to 0.4 mag at about 100 days when we stop the light-curve calculation.

### 2.3. Spectra

Finally, detailed NLTE spectra have been constructed based on the high-curve calculations. Thus, the effect of energy stored during previous epochs is properly taken into account. The energetics of the model are calculated. Given an explosion model, the evolution of the spectrum is not subject to any tuning or free parameters such as the total luminosity. A modified version of our code for NLTE extended atmospheres (NEATs) is used. Although time dependence in the rate equations can be included in this code, it has been omitted because it was found to be negligible. For details see Höflich (1990, 1995) and Höflich et al. (1997) and references therein.

For the NLTE spectra, the density, chemical profiles, and the luminosity as a function of the radial distance  $r$  are given by the hydrodynamical explosion and the light-curve calculations, including the Monte Carlo scheme for  $\gamma$ -ray transport. The radiation transport equation (including relativistic terms) is solved in the comoving frame according to Mihalas, Kunacz, & Hummer (1975, 1976a, 1976b). Blocking by weak lines is included in a “quasi” continuum approximation; i.e., the frequency derivative terms in the

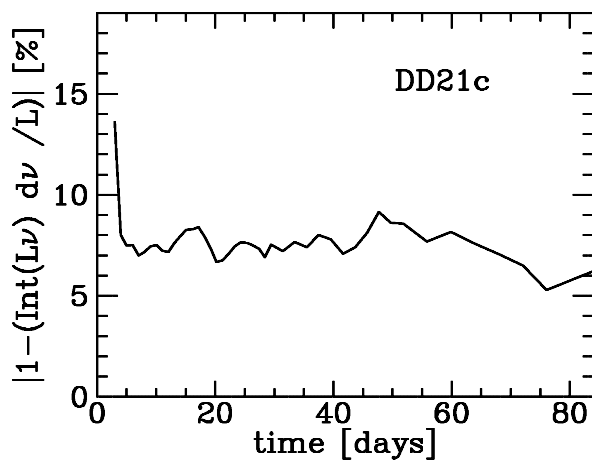


FIG. 2.—Test for the consistency of the integrated luminosity based on the solution of the monochromatic and frequency-integrated radiation transport equation for model DD21c (Table 1). About 780 frequencies have been used in the former case. Note that this inconsistency involves only the Eddington factors, which are based on the solution of the monochromatic transport equation, but not the energy conservation.

radiation transport equation are included in the narrow-line limit to calculate the probability for photons to pass a radial subshell along a given direction  $\mu$  (Castor 1974; Abbot & Lucy 1985; Höflich 1990). The statistical equations are solved consistently with the radiation transport equation to determine the LTE occupation numbers using both an accelerated  $\Lambda$  iteration (see Olson, Auer, & Buchler 1986) and an equivalent–two-level approach for transitions from the ground state. That provides an efficient way to take the nonthermal fraction of the source function into account during the radiation transport and, effectively accelerates both the convergence rate and the stability of the systems (Höflich 1990, 1995). A comparison of the explicit with the implicit source functions provides a sensitive tool to test for convergence of the system of rate and radiation transport equations.

Excitation by  $\gamma$ -rays is included. Detailed atomic models are used for up to the three most abundant ionization stages of several elements, i.e., C, O, Ne, Na, Mg, Si, S, Ca, Fe, Co, Ni, taking into account 20–30 levels and 80–180 transitions in the main ionization stage. Here, we use detailed term schemes for C II, O II, Ne I, Na I, Mg II, Si II, S II, Ca II, Fe II, Co II, and Ni II. The corresponding lower and upper ions are represented by the ground states. The energy levels and cross sections of bound-bound transitions are taken from Kurucz (1993a, 1993b, 1996). In addition to  $\approx 10,000$  lines treated in full NLTE, a total of  $\approx 10^6$  lines out of a list of  $31 \times 10^6$  (Kurucz 1993a) are included for the radiation transport. For these lines, we assume LTE population numbers for each ion. To calculate the ionization balance, excitation by hard radiation is taken into account. LTE-line scattering is not taken as a free parameter (Nugent et al. 1997). Instead, LTE-line scattering is included using an equivalent–two-level approach, calibrated by the elements treated in full NLTE.

## 3. RESULTS

### 3.1. Explosion Models

The influence of the initial metallicity and mixing on light curves and spectra has been studied for the example of a set of delayed detonation models using DD21c as the reference model. In Table 1, the quantities given in columns (2)–(9) are as follows  $M_*$  = WD mass;  $\rho_c$  = central density of the WD (in  $10^9 \text{ g cm}^{-3}$ );  $\alpha$ -ratio of the deflagration velocity and local sound speed;  $\rho_{tr}$  transition density (in  $10^7 \text{ g cm}^{-3}$ ) at which the deflagration is assumed to turn into a detonation; C/O ratio;  $R_Z$  = the metallicity relative to solar by mass;  $E_{kin}$  = kinetic energy (in  $10^{51}$  ergs);  $M_{Ni}$  = mass of  $^{56}\text{Ni}$  (in solar units). The parameters are close to those that reproduce both the spectra and light curves reasonably well (Nomoto, Thielemann, & Yokoi 1984; Höflich 1995; Höflich & Khokhlov 1996).

TABLE 1  
BASIC PARAMETERS FOR THE DELAYED DETONATION MODELS

Model	$M_*$	$\rho_c$	$\alpha$	$\rho_{tr}$	C/O	$R_Z$	$E_{kin}$	$M_{Ni}$
DD13c.....	1.4	2.6	0.03	3.0	1/1	1/1	1.36	0.79
DD21c.....	1.4	2.6	0.03	2.7	1/1	1/1	1.32	0.69
DD23c.....	1.4	2.6	0.03	2.7	2/3	1/1	1.18	0.59
DD24c.....	1.4	2.6	0.03	2.7	1/1	1/3	1.32	0.70
DD25c.....	1.4	2.6	0.03	2.7	1/1	3/1	1.32	0.69
DD26c.....	1.4	2.6	0.03	2.7	1/1	1/10	1.32	0.73
DD27c.....	1.4	2.6	0.03	2.7	1/1	10/1	1.32	0.69

TABLE 2  
TOTAL ABUNDANCES OF  
MODEL DD21c WITH  
SOLAR INITIAL  
COMPOSITION

Element	Abundance
He .....	1.16E-03
C .....	5.44E-04
O .....	5.03E-02
Ne .....	1.67E-03
Na .....	1.05E-05
Mg .....	1.02E-02
Al .....	6.12E-05
Si .....	2.06E-01
P .....	2.30E-05
S .....	1.49E-01
Cl .....	9.50E-06
Ar .....	3.56E-02
K .....	7.50E-06
Ca .....	4.00E-02
V .....	1.02E-03
Cr .....	2.20E-02
Mn .....	1.44E-02
Fe .....	6.87E-01
Co .....	1.28E-02
Ni .....	2.19E-02
Cu .....	1.61E-05

To study the influence of a variation of the C/O ratio, a model (DD23c) with the same parameters as DD21c has been constructed, but with  $C/O = \frac{2}{3}$  by abundance. The total abundances of the most important elements are given for the reference model DD21c in Table 2. Figure 3 gives the density and velocity versus mass for the reference model DD21c, a model with a higher transition density (DD13c), and a model with reduced C/O ratio (DD23c). Figure 4 gives the composition profiles of the major elements for the same three models. The overall density and velocity structures are insensitive to the transition density and to the C/O ratio. Qualitatively, the final burning products can be

understood by the relation between hydrodynamical and individual nuclear timescales. The hydrodynamical timescale is given by the total energy release during the burning of the progenitor. Since most of the energy is released by the explosive burning of carbon and oxygen, the energy production per gram depends on the initial chemical composition of the WD, i.e., the C/O ratio. The nuclear timescales are determined by the peak temperature during burning, which depends on the energy release per unit volume because the energy density is radiation dominated. As the energy release per gram is fixed, the peak temperature is given by the composition and the local density. Thus, the latter two are the dominant factors for the final composition of a zone. With decreasing transition density, less  $^{56}\text{Ni}$  is produced and the intermediate-mass elements expand at lower velocities because the later transition to detonation allows for a longer preexpansion of the outer layers (DD21c vs. DD13c). Similarly, with a decreasing C/O ratio in the progenitor, the specific energy release during the nuclear burning is reduced (DD23c vs. DD21c) and the transition density is reached later in time, resulting in a larger preexpansion of the outer layers and a narrower region dominated by Si. Moreover, a change of the C/O ratio from 1 to  $\frac{2}{3}$  reduces the  $^{56}\text{Ni}$  production by about 20%. The kinetic energy is reduced by 10% corresponding to a 5% change in the mean expansion velocity. To first approximation a reduction in the transition density has a similar effect to a decrease of the C/O ratio or a reduction of the central density (Höflich & Khokhlov 1996).

To test the influence of the metallicity for  $Z \geq 20$  (i.e., nuclei beyond Ca) we have constructed models with parameters identical to DD21c but with initial metallicities between 0.1 and 10 times solar (Table 1). The energy release, density, and velocity structure are virtually identical to that of DD21c. The main difference is a slight increase in the  $^{56}\text{Ni}$  mass with decreasing metallicity due to a higher  $Y_e$ . The reason is that the metallicity mainly affects the initial

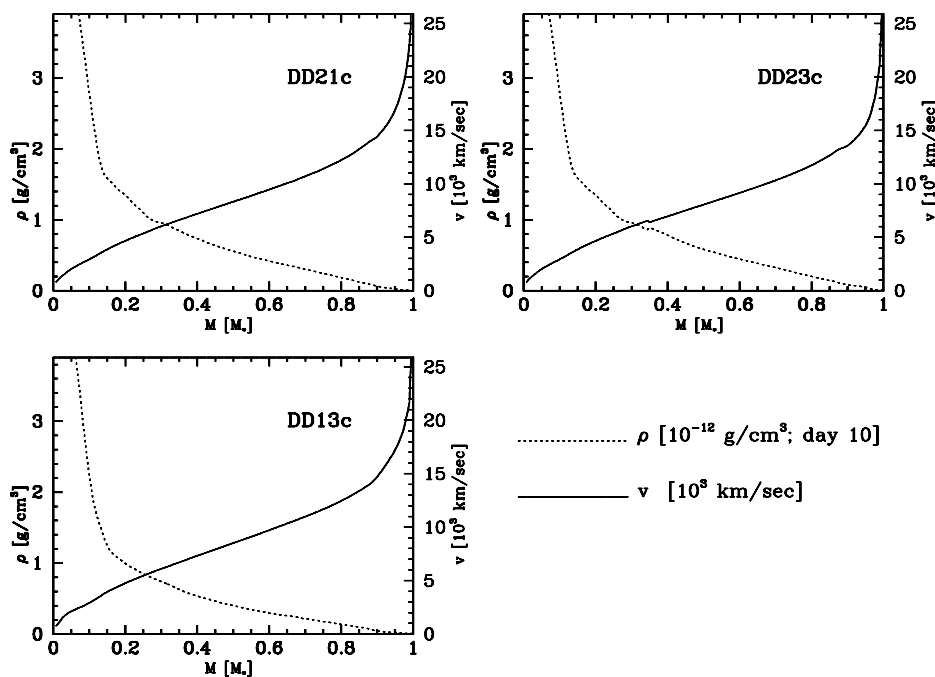


FIG. 3.—Density and velocity as a function of mass for three delayed detonation models (Table 1)

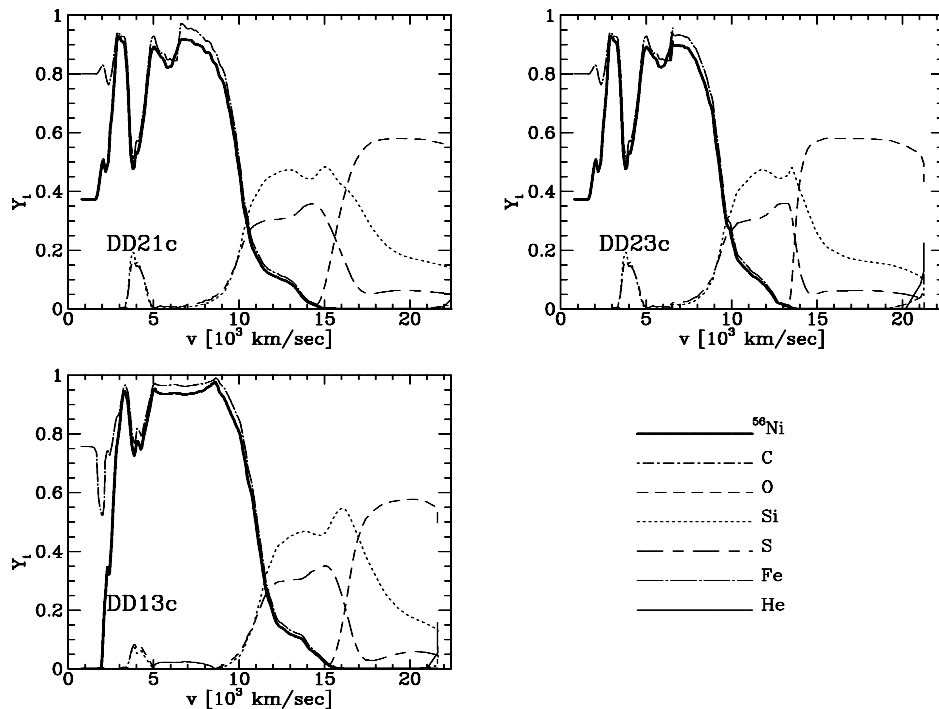


FIG. 4.—Abundances as a function of the final expansion velocity for the three delayed detonation models of Fig. 3. Both the initial  $^{56}\text{Ni}$  and the final Fe profiles are shown.

CNO abundances of a star. These are converted during the preexplosion stellar evolution to  $^{14}\text{N}$  in H burning and via  $^{14}\text{N}(\alpha, \gamma)^{18}\text{F}(\beta^+)^{18}\text{O}(\alpha, \gamma)^{22}\text{Ne}$  to nuclei with  $N = Z + 2$  in He burning. The result is that increasing metallicity yields a smaller proton-to-nucleon ratio ( $Y_e$ ) throughout the preexplosive WD (Thielemann et al. 1997). Higher metallicity and smaller  $Y_e$  lead to the production of more neutron-rich iron group nuclei and less  $^{56}\text{Ni}$ . For lower metallicity, and thus higher  $Y_e$ , some additional  $^{56}\text{Ni}$  is produced at the expense of  $^{54}\text{Fe}$  and  $^{58}\text{Ni}$  (Thielemann, Nomoto, & Yokoi 1986). The temperature in the inner layers is sufficiently high during the explosion that electron capture determines  $Y_e$ . In those layers, the initial metallicity has no influence on the final burning product. The total production of isotopes of all the models is given in Table 3. Figure 5 gives the distribution of various isotopes in models DD21c, DD24c, and DD27c, which represent solar  $\frac{1}{3}$  solar and 10 times solar metallicities, respectively. The main differences due to changes in  $Z$  are in regions with expansion velocities in excess of  $\approx 12,000 \text{ km s}^{-1}$ . Most remarkable is the change in the  $^{54}\text{Fe}$  production, which is the dominant contributor to the abundance of iron group elements at these velocities, since little cobalt has yet been decayed near maximum light. For increasing metallicity, the production of this isotope increases significantly. For  $\frac{1}{3}$  solar metallicity, hardly any  $^{54}\text{Fe}$  is produced at high velocities, but  $^{54}\text{Fe}$  is as high as 5% by mass fraction if we start with 10 times the solar metallicity. We note that these layers with  $v \geq 12,000 \text{ km s}^{-1}$  dominate the spectra around maximum light, and lines of iron group elements are an important contributor to the line opacities (see below).

### 3.2. Light Curves

As discussed in previous papers (e.g., Höflich et al. 1997 and references therein), bolometric and monochromatic

light curves provide a valuable tool to probe the underlying explosion models, namely, the absolute amount of  $^{56}\text{Ni}$  and its distribution.

Bolometric and monochromatic light curves are shown in Figures 6 and 7. Reducing the C/O ratio from 1/1 to 2/3 in the WD reduces the  $^{56}\text{Ni}$  production and the kinetic energy in DD23c compared to DD21c. Both the bolometric and monochromatic light curves are affected. The smaller expansion due to the smaller  $E_{\text{kin}}$  causes a reduced geometrical dilution of the matter and a reduction of the expansion work at a given time. Consequently, for reduced C/O ratios, the rise time to maximum light is slower by about three days and the maximum brightness is larger because more of the stored energy goes into the radiation rather than into kinetic energy. The reduced heating at the later time of maximum light also implies that DD23c is slightly redder [ $\Delta(B - V) \approx 0.02 \text{ mag}$ ] than DD21c at its peak. After about day 35, however, the luminosity is smaller by about 10% for the lower C/O ratio because of smaller  $^{56}\text{Ni}$  production (i.e., the instantaneous energy production). The postmaximum decline is steeper. The change of the C/O ratio from 1/1 to 2/3 has a similar effect on the colors, the light-curve shape, and the distribution of elements to that of a 10% reduction of the transition density or of the central density in delayed detonations. For a given ratio of peak to tail, a model produced by a reduced C/O ratio will be brighter than one obtained by varying the transition density (Höflich 1995). The rise time and the expansion rate as measured by the Doppler shift of lines (see below) provide a way to determine the C/O ratio and the transition density independently (Table 2; compare Khokhlov et al. 1993; Höflich 1995; Höflich & Khokhlov 1996). The current state of the art for light-curve calculations and for the progenitor evolution does not allow for a sufficiently fine discrimination to determine the absolute C/O ratio. A careful differ-

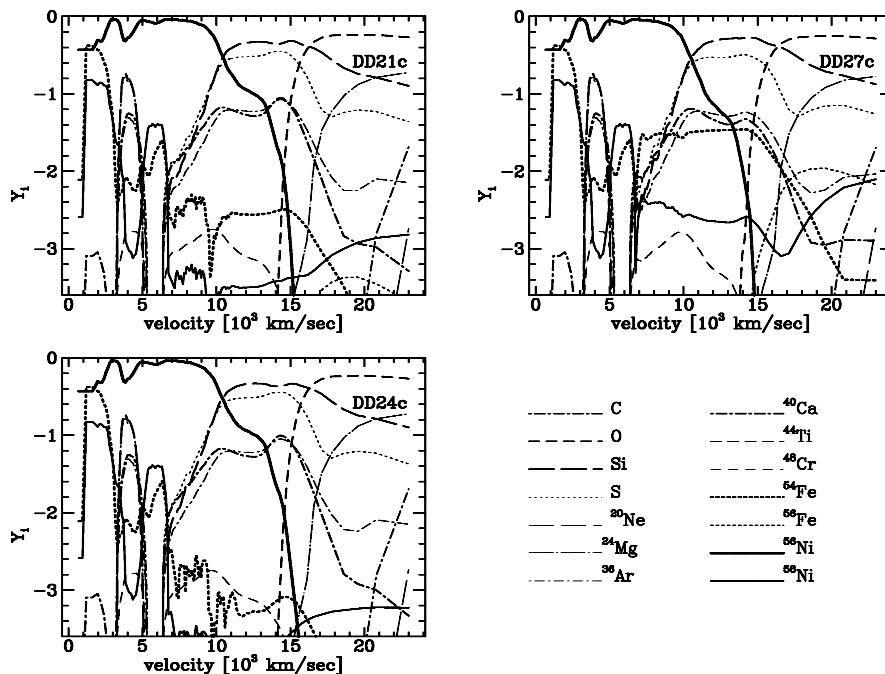


FIG. 5.—Abundances of different isotopes as a function of the expansion velocity for models DD21c, DD24c, and DD27c that have initial compositions of solar, 1/3 solar, and 1/10 solar, respectively.

ential analysis of observations may yield information on the relative variation of the C/O ratio, and the central ignition density or transition density.

Changing the initial metallicity  $Z$  has very little influence on the bolometric light curve (compare DD21c, DD24 in Fig. 6) because the  $^{56}\text{Ni}$  production and energy release vary by only 4% over the entire range of models. In addition, diffusion timescales are mainly determined by deeper layers that are unaffected by  $Z$ .

Monochromatic light curves are slightly more affected by changes in the initial metallicity  $Z$  (Fig. 7, upper panel). The principal effect is that the radiative cooling in the outer layers increases with  $Z$ . Consequently, depending on the

phase,  $B-V$  is larger and redder by about 0.02–0.04 mag. The absolute brightness varies by about the same amount. The time of maximum light shifts by only  $\approx 1$  day.

### 3.3. Spectra at Maximum Light

Variations in the pattern of the most abundant elements is similar for changes in the C/O ratio, the transition density, and the central density of the WD (see Figs. 3 and 4). Consequently, the variation of the spectra as a result of changing these parameters is similar. Differences would show up in correlation between light-curve shape and Doppler shifts of lines at a given phase (see above).

The influence of the initial metallicity  $Z$  is interesting primarily because it influences the iron group elements. As an example, the spectra of the delayed detonation models with solar and  $\frac{1}{3}$  solar metallicity are given in Figure 8. At maximum light ( $\approx 17$  days), the line-forming region ( $\tau \approx 0.1, \dots, 1.0$ ) extends between  $1$  and  $2 \times 10^{15}$  cm in the optical (Fig. 8, lower graph), corresponding to expansion velocities between 8000 and 16,000  $\text{km s}^{-1}$ . In this velocity range the material has been subjected to at least partial oxygen burning to silicon, and the deeper layers are rich in  $^{56}\text{Ni}$ . This means that the iron peak elements visible in the optical spectrum near maximum light are freshly synthesized and do not directly represent the initial metallicity. The initial metallicity does affect the optical spectrum near maximum, but only indirectly and only in the blue. The abundances of the intermediate-mass elements are not affected by the metallicity, but the abundance of  $^{54}\text{Fe}$  is a sensitive function of the initial  $Z$ , and  $^{54}\text{Fe}$  provides an important source of Fe lines to the opacity for the matter with  $v \gtrsim 10,000$   $\text{km s}^{-1}$ . The iron line opacity is most substantial for wavelengths less than  $\sim 4000$  Å. The effect of the initial metallicity on the spectrum can be seen in the wavelength region  $\sim 3000$  Å in Figure 8 (top). The initial metallicity might be directly observed by examination of UV

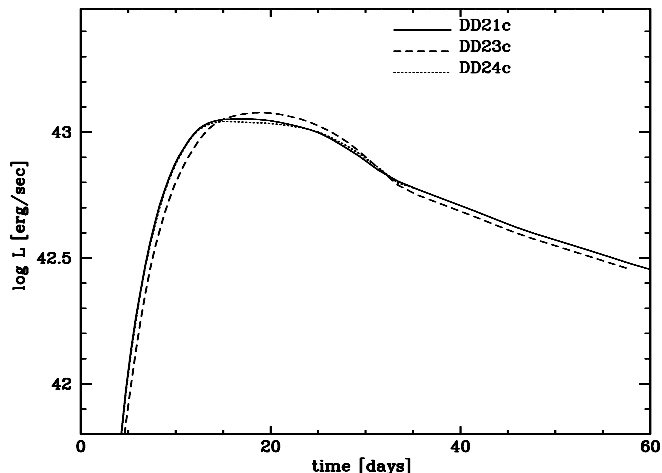


FIG. 6.—Comparison of bolometric light curves of the delayed detonation models DD21c, DD23c, and DD24c with otherwise identical parameters but with different C/O ratios and metallicity relative to solar (C/O;  $R_z$ ) of (1; 1), ( $\frac{2}{3}$ ; 1) and (1; 0.3), respectively.

TABLE 3  
 PRODUCTION OF ISOTOPES  $M_i$  IN  $M_\odot$  WITH  $M_i \geq 1E-10$  FOR DELAYED DETONATION MODELS (SEE TABLE 1)

Isotope	DD21c	DD13c	DD23c	DD24c	DD25c	DD26c	DD27c
<sup>4</sup> He.....	1.16E-03	7.33E-03	2.58E-03	1.16E-03	1.16E-03	1.16E-03	1.16E-03
<sup>12</sup> C.....	5.44E-04	3.50E-04	1.04E-03	5.38E-04	5.39E-04	5.40E-04	5.33E-04
<sup>15</sup> N.....	6.52E-09	7.20E-09	8.09E-09	1.78E-08	2.18E-09	4.66E-08	5.38E-10
<sup>16</sup> O.....	5.03E-02	4.65E-02	6.80E-02	4.98E-02	5.01E-02	4.99E-02	4.88E-02
<sup>20</sup> Ne.....	1.67E-03	1.54E-03	2.06E-03	1.67E-03	1.65E-03	1.68E-03	1.61E-03
<sup>21</sup> Ne.....	1.27E-08	6.35E-09	2.22E-08	1.16E-08	1.43E-08	1.12E-08	1.82E-08
<sup>22</sup> Ne.....	2.21E-08	1.13E-08	4.18E-08	2.39E-08	1.86E-08	2.47E-08	1.56E-08
<sup>23</sup> Ne.....	1.05E-05	7.68E-06	1.36E-05	1.02E-05	1.12E-05	1.01E-05	1.22E-05
<sup>24</sup> Mg.....	1.02E-02	1.09E-02	1.54E-02	1.02E-02	1.00E-02	9.52E-03	9.36E-03
<sup>25</sup> Mg.....	8.09E-07	8.47E-07	1.59E-06	2.77E-07	1.20E-06	1.57E-07	1.95E-06
<sup>26</sup> Mg.....	6.26E-07	5.01E-07	8.89E-07	4.18E-07	1.23E-06	3.17E-07	3.21E-06
<sup>27</sup> Al.....	6.12E-05	6.62E-05	7.68E-05	4.90E-05	1.01E-04	5.03E-05	1.68E-04
<sup>28</sup> Si.....	2.06E-01	1.65E-01	2.12E-01	2.07E-01	2.09E-01	2.08E-01	2.11E-01
<sup>29</sup> Si.....	7.67E-05	8.40E-05	1.17E-04	4.84E-05	1.03E-04	3.15E-05	1.43E-04
<sup>30</sup> Si.....	3.10E-05	1.83E-05	1.83E-05	7.69E-05	2.12E-05	1.11E-04	7.63E-05
<sup>31</sup> P.....	2.30E-05	1.79E-05	2.74E-05	3.71E-05	2.41E-05	6.01E-05	4.74E-05
<sup>32</sup> S.....	1.49E-01	1.12E-01	1.53E-01	1.53E-01	1.46E-01	1.56E-01	1.39E-01
<sup>33</sup> S.....	5.25E-05	3.79E-05	7.45E-05	3.57E-05	6.91E-05	2.53E-05	1.03E-04
<sup>34</sup> S.....	2.19E-05	2.03E-05	1.83E-05	2.66E-05	8.66E-05	3.96E-05	3.43E-04
<sup>35</sup> Cl.....	9.50E-06	6.33E-06	1.60E-05	1.17E-05	1.45E-05	1.80E-05	3.14E-05
<sup>36</sup> Ar.....	3.56E-02	2.60E-02	3.74E-02	3.70E-02	3.41E-02	3.80E-02	3.11E-02
<sup>37</sup> Cl.....	7.75E-06	4.31E-06	1.22E-05	5.63E-06	9.62E-06	3.94E-06	1.44E-05
<sup>38</sup> Ar.....	1.28E-05	1.09E-05	1.23E-05	8.52E-07	6.95E-05	1.03E-06	2.64E-04
<sup>39</sup> K.....	7.50E-06	4.24E-06	2.34E-05	3.31E-06	1.54E-05	3.82E-06	3.05E-05
<sup>40</sup> Ca.....	4.00E-02	2.94E-02	4.23E-02	4.19E-02	3.77E-02	4.30E-02	3.34E-02
<sup>41</sup> Ca.....	1.87E-06	8.10E-07	5.84E-06	1.31E-06	2.43E-06	9.25E-07	3.90E-06
<sup>42</sup> Ca.....	2.95E-07	1.89E-07	6.00E-07	8.80E-09	1.63E-06	9.36E-09	6.71E-06
<sup>43</sup> Ca.....	6.33E-09	5.62E-08	4.59E-07	9.07E-09	6.47E-09	1.84E-08	1.41E-08
<sup>44</sup> Ca.....	3.04E-05	3.65E-05	8.38E-05	3.13E-05	2.92E-05	3.18E-05	2.73E-05
<sup>45</sup> Sc.....	1.56E-07	7.57E-08	3.08E-06	1.42E-07	1.84E-07	1.18E-07	2.46E-07
<sup>46</sup> Ca.....	2.60E-09	2.36E-09	4.21E-09	6.14E-10	8.54E-09	1.75E-10	2.11E-08
<sup>48</sup> Ca.....	9.43E-09	8.07E-09	1.44E-08	3.15E-09	2.76E-08	9.59E-10	8.74E-08
<sup>46</sup> Ti.....	3.03E-07	4.15E-06	8.37E-06	1.37E-07	1.00E-06	1.24E-07	4.15E-06
<sup>47</sup> Ti.....	4.55E-07	3.94E-06	1.96E-05	4.41E-07	4.99E-07	4.49E-07	6.62E-07
<sup>48</sup> V.....	1.02E-03	7.92E-04	1.63E-03	1.03E-03	9.80E-04	1.04E-03	8.92E-04
<sup>49</sup> V.....	2.75E-05	1.92E-05	2.04E-04	2.37E-05	3.46E-05	1.87E-05	4.62E-05
<sup>50</sup> Cr.....	8.73E-05	9.16E-05	6.91E-04	7.69E-05	1.27E-04	7.49E-05	2.70E-04
<sup>51</sup> Cr.....	1.23E-04	3.17E-05	1.38E-03	1.16E-04	1.39E-04	1.16E-04	1.70E-04
<sup>52</sup> Cr.....	2.20E-02	1.57E-02	2.83E-02	2.21E-02	2.15E-02	2.20E-02	2.02E-02
<sup>50</sup> Mn.....	6.96E-07	5.64E-07	1.49E-05	6.97E-07	6.95E-07	7.03E-07	6.94E-07
<sup>53</sup> Mn.....	1.07E-03	7.17E-04	4.25E-03	9.71E-04	1.26E-03	9.16E-04	1.60E-03
<sup>54</sup> Mn.....	3.42E-09	6.65E-07	7.82E-07	1.68E-09	2.17E-08	1.63E-09	1.49E-07
<sup>55</sup> Mn.....	1.44E-02	4.21E-03	3.41E-02	1.40E-02	1.54E-02	1.38E-02	1.72E-02
<sup>54</sup> Fe.....	4.17E-02	4.84E-02	6.83E-02	4.04E-02	4.65E-02	4.00E-02	6.22E-02
<sup>56</sup> Fe.....	6.87E-01	7.75E-01	5.63E-01	6.89E-01	6.83E-01	6.97E-01	6.79E-01
<sup>57</sup> Co.....	1.28E-02	9.43E-03	1.83E-02	1.27E-02	1.33E-02	1.26E-02	1.45E-02
<sup>58</sup> Ni.....	2.19E-02	2.58E-02	3.05E-02	2.18E-02	2.24E-02	2.17E-02	2.41E-02
<sup>59</sup> Ni.....	1.34E-04	9.92E-04	2.95E-04	1.29E-04	1.46E-04	1.28E-04	1.82E-04
<sup>60</sup> Cu.....	1.61E-05	9.04E-03	1.65E-05	1.63E-05	1.60E-05	1.67E-05	1.60E-05
<sup>61</sup> Cu.....	1.95E-06	3.85E-04	4.91E-06	1.93E-06	1.99E-06	1.92E-06	2.04E-06
<sup>62</sup> Cu.....	4.17E-06	3.12E-04	3.70E-06	4.17E-06	4.17E-06	4.16E-06	4.17E-06
<sup>63</sup> Zn.....	3.66E-08	1.66E-03	9.42E-08	3.42E-08	3.61E-08	3.17E-08	3.33E-08
<sup>64</sup> Zn.....	9.62E-08	5.25E-03	2.10E-07	3.15E-08	2.69E-07	1.23E-08	8.54E-07
<sup>65</sup> Zn.....	1.49E-08	2.28E-05	1.85E-08	4.27E-09	4.61E-08	1.27E-09	1.33E-07
<sup>66</sup> Ga.....	2.16E-09	6.81E-06	2.94E-09	1.16E-09	3.83E-09	7.72E-10	5.68E-09
<sup>67</sup> Ge.....	1.55E-09	4.96E-06	1.85E-09	7.79E-10	1.86E-09	2.65E-10	1.17E-09

spectra that form in the outermost layers with  $v \gtrsim 16,000\text{--}17,000 \text{ km s}^{-1}$ , and that have not been subject to oxygen burning.

By two to three weeks after maximum, the spectra are completely insensitive to the initial  $Z$  because the spectrum is formed in even deeper layers where none of the important abundances are affected by the metallicity. Thus, for two similar bright SNe with similar expansion velocities, a comparison between their spectral evolutions can provide a method to determine the metallicity difference, or may be used to detect evolutionary effects for distant SNe Ia (see below).

Note that the UV spectra may provide a unique tool to probe the very outer layers, which may have undergone little burning during the explosion.

#### 3.4. Mixing during the Explosion

Until now we have omitted a potential difficulty involved in the determination of  $Z$ . As already mentioned, we may see strong iron group elements in the line-forming region near maximum because they are produced at high velocities. Alternatively, these elements may be mixed out during the explosion, but after burning has taken place. To test this, we have artificially mixed the composition but kept the

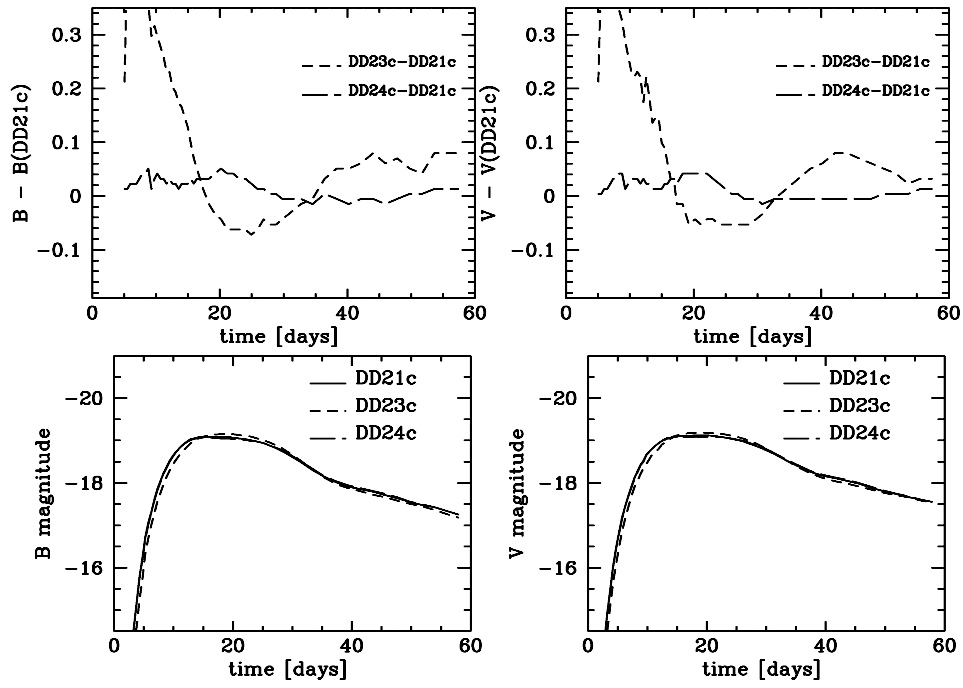


FIG. 7.—Comparison of light curves in  $B$  (left) and  $V$  (right) of the delayed detonation models DD21c, DD23c, and DD24c with otherwise identical parameters but different C/O ratios and metallicities relative to solar (C/O;  $R_Z$ ) of (1; 1), ( $\frac{2}{3}$ ; 1), and (1;  $\frac{1}{3}$ ). The differences relative to DD21c and the monochromatic light curves are given in the upper and lower plots, respectively.

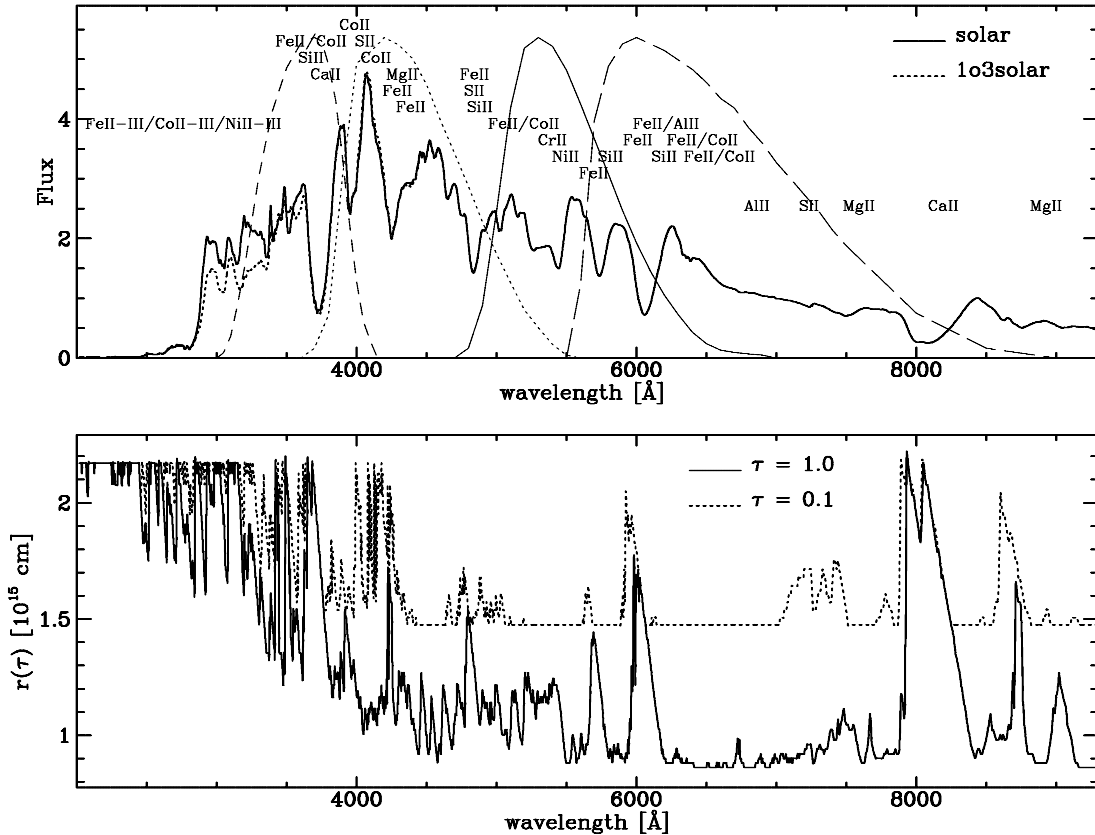


FIG. 8.—Comparison of synthetic NLTE spectra at maximum light for initial compositions of solar and  $\frac{1}{3}$  solar (1o3), respectively, for model DD21c (upper graph). The standard Johnson filter functions for  $UBVR$  and  $R$  are also shown. In the lower graph, the radius as a function of wavelength where the monochromatic optical depth reaches 0.1 and 1, respectively, is given for DD21c.

overall structure fixed (see Fig. 9). Unlike a change in the initial metallicity, mixing alters the entire spectrum. All burning products will be enhanced in the outer region, including Ni, Co, and Ca. In particular, the Ca lines at about 4000 Å and in the IR triplet provide a way to distinguish mixing from metallicity effects.

#### 4. IMPLICATIONS FOR COSMOLOGY

Systematic effects that must be taken into account in the use of SNe Ia to determine cosmological parameters include technical problems, changes in the environment with time, changes in the statistical properties of the SNe Ia, and changes in the physical properties of SNe Ia, which are the main subject of this study. The estimates given below of the redshifts when evolutionary effects become important are based on the assumptions (!) of a flat universe with an age of 14 Gyr and of evolution timescales for the progenitors of about 0.5–6 Gyr, which are given by the zero-age main sequence (ZAMS) lifetimes of Population II donor stars with masses between 1 and 7  $M_{\odot}$  (Schaller et al. 1992).

In the first class of technical problems, we put corrections for redshift. If standard filter systems are used, they can be well calibrated to local standards but the  $k$ -correction is of some concern. This problem can be overcome if redshifted “standard” filters are used. Another technical problem may then arise from the fact that the transmission functions must be identical to those resulting from the redshift because no direct calibration can be applied by using a comparison star.

In the second class of problems associated with the environment is the important fact that the properties of dust may change at high redshift. In the first place, the element abundances in the interstellar medium (ISM) can change. In addition, important donors of dust such as low-mass red giant stars cannot contribute because their evolutionary time is comparable to, or longer than, the age of the universe at  $z \approx 0.5$ –1. Another problem related to the correction for extinction is that the application of the extinction law depends on the redshift of the absorbing dust cloud. For details see Höflich & Khokhlov (1996).

In the third class of problems related to the statistical properties is the fact that the contribution of different progenitor types may change with redshift. For local supernovae, it is likely that a large variety of binary star properties (total mass of donor stars, separation, etc.) with

very different evolutionary lifetimes account for the variety of SNe Ia observed (Höflich et al. 1997). Given this variety, we expect a time evolution of the statistical properties of the progenitors because, early on, progenitors with short lifetimes will dominate the sample. Among other changes, more massive, shorter lifetime progenitors will have a lower C/O ratio in the center (see below). Changes in the statistical properties are expected to increase substantially at redshifts larger than 0.7–0.8, where the age of the universe becomes comparable to, or shorter than, the suspected progenitor lifetimes. Other evolutionary effects have been mentioned in the introduction: The ZAMS lifetime changes with metallicity, Roche lobe radii change with metallicity, and the lower limit for accretion and steady burning of hydrogen on the surface of the WD changes by a factor of 2 between Population I and Population II stars (Nomoto et al. 1997).

Finally, the properties of the typical, individual SNe Ia may change. If more massive stars contribute to the supernova population, we expect a smaller C/O ratio. Changing the C/O ratio from 1/1 to 2/3 with otherwise identical parameters (see § 3.2) will result in a smaller  $^{56}\text{Ni}$  production and, consequently, a lower bolometric luminosity at late times. On the other hand, the slower expansion causes less adiabatic cooling during early times, and thus the luminosity at maximum light is larger (Fig. 6). This implies that the peak-to-tail luminosity ratio changes with the C/O ratio. The consequence for analyses that use light-curve shapes or the postmaximum decline (e.g.,  $\delta m_{15}$ ) is evident. Quantitatively, for the monochromatic light curves in our example, the difference in the peak-to-tail luminosity ratio is  $\approx 0.1, \dots, 0.2$  mag. For techniques to determine the absolute peak luminosity by measuring either  $\delta m_{15}$  or light-curve shapes (e.g., Hamuy et al. 1996; Riess et al. 1995), this translates into a systematic error of  $\approx 0.3$  mag in  $m_v$ . This systematic change in peak luminosity with redshift due to changing C/O ratios could mimic the effects of cosmology. Note that the transition density from deflagration to detonation may depend on the energy release during the deflagration phase, and hence the transition density could be a function of the C/O ratio. Both effects could alter the light curve.

The other physical effect on the SNe Ia themselves is the influence of the initial metallicity  $Z$  on the nuclear burning conditions during the explosion. This produces a change of

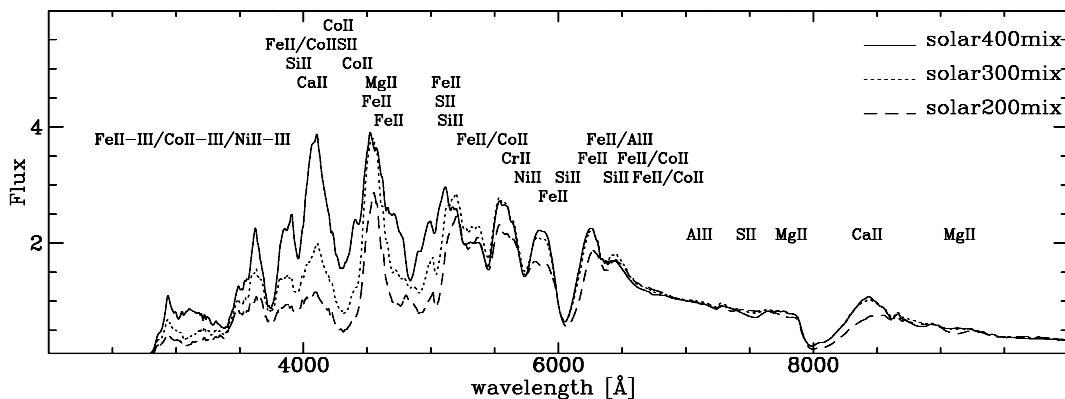


FIG. 9.—Comparison of synthetic spectra at maximum light assuming complete mixing of the outer layers, involving 64% (solar 200 mix), 48% (solar 300 mix) and 24% (solar 400 mix) of the total mass, respectively (see Figs. 3 and 4).

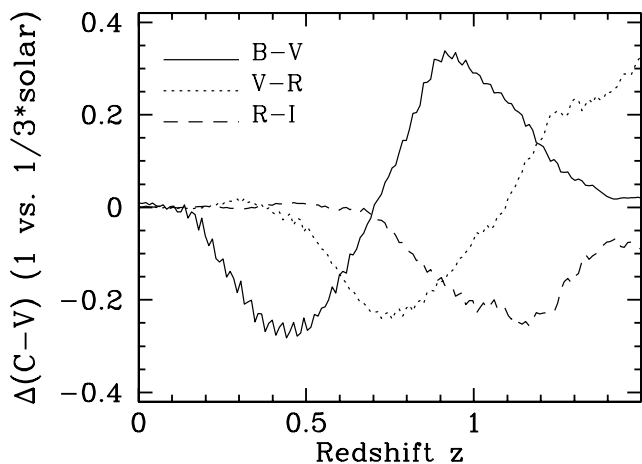


FIG. 10.—Metallicity effect on  $B-V$  and  $R-V$  for DD21c as a function of the redshift.

the isotopic composition in the outer layers. A reduction of  $Z$  with redshift  $z$  is expected. Note that the metallicity corresponds to the redshift when the progenitor is formed and not the redshift when the SN Ia is observed. Although small, the changes in the spectrum with metallicity have an important effect on the colors of SNe at high redshifts where they are shifted into other bands (see Fig. 10). For local SNe Ia, a change of the metallicity by a factor of 3 implies a variation in color of 0.02–0.03 mag. For  $z \geq 0.2$  however, Figure 10 shows that such a change can induce a systematic change in  $B-V$  of up to 0.3 mag. For  $V-R$  and  $R-I$ , the effect remains small for redshifts  $z \leq 0.5$  and 0.7, respectively, but it increases to the same order at redshifts relevant for the determination of cosmological parameters. The amplitude of this effect and hence the uncertainty in color, reddening, and brightness with metallicity is again comparable to the brightness change imposed by cosmological deceleration.

If SNe at moderate ( $\approx 0.5$ ) and high ( $\approx 1.0$ ) redshifts are used to determine  $\Omega_M$  and  $\Omega_\Lambda$ , respectively, these systematic shifts, changes of the amplitude of the variation with redshift and the influence of the metallicity on the color indices, may prevent a proper determination of the cosmological parameters if it is not taken into account. Because of the effect of metallicity on color and the different timescales for progenitor evolution and also the statistical properties discussed above, the distribution of peak brightness as a function of light-curve shape and redshift is likely to produce a scatter in the distribution of the cosmological parameters. The way to reduce this scatter is to understand its physical origin in the sorts of effects we have outlined here. Detailed spectral analyses of different SNe may show that the effects of metallicity remain moderate (even today all progenitors may have a low  $Z$ ) or that it can be corrected by using models. Quantitatively, other dynamical models and metal-

licities will give different amplitudes of  $\Delta(B-V)$ ,  $\Delta(V-R)$ , and  $\Delta(R-I)$  at a given  $z$  than those illustrated. In general, the use of redshifted filters will eliminate the major systematic effect illustrated in Figure 10, but even putting aside the systematic problems due to the realization of identical transmission functions, the small “noise” (see Fig. 10) due to the “bumpy” spectra is real and requires a very narrow grid of filters with respect to redshift. Otherwise, the determinations of  $q_0$  will show a significant intrinsic spread. Even if corrections for redshift and the small wiggles are applied, and if corrections for the interstellar reddening are determined, a systematic effect of the order of 0.1 mag will remain because of the small but systematic dependencies in the color indices at  $z = 0$  (see Fig. 10).

In conclusion, both the change of  $Z$  and the C/O ratio in the progenitor may be expected to give variations in the peak brightness derived of the order of a few tenths of a magnitude as one goes from  $z \approx 0$  to  $z \approx 1$ . As a guideline, we give in Table 4 the size of the systematic effects as they enter  $q_0$ ,  $\Omega_M$  and  $\Omega_\Lambda$  to first order for Friedmann-Lemaître cosmological models (Goodbar & Perlmutter 1996; Perlmutter et al. 1997) for which  $q_0 = \Omega_M/2 - \Omega_\Lambda$  with  $\Omega_\Lambda = \Lambda/(3H_0^2)$  and, for a flat universe,  $\Omega_M + \Omega_\Lambda = 1$ . To first order, the uncertainties are proportional to  $1/z$  and  $\Delta m$ . An uncertainty  $\Delta m = 0.6$  mag should be regarded as the worst-case scenario. At this point, a warning is appropriate. Although the assumed size of the change in the initial metallicity  $Z$  is of the right order based on the chemical evolution of galaxies (Samland, Hensler, & Theis 1997), metallicity change as a function of galactic evolution is highly uncertain. Yet another uncertainty enters because  $Z$  is set by the time the progenitor is born, and there can be a large range of times before the star dies. Moreover, the statistical properties of progenitor systems are not well known. For instance, the mass of the progenitors and the donor stars must be in the range between  $\approx 1$  and  $7 M_\odot$ , but the relative contributions within this mass range are unknown even for local SNe Ia. To beat down these uncertainties, comparative analyses of the light curves and spectra (e.g., velocities, line shifts, spectral flux distributions) of both the local and distant SNe Ia are required.

## 5. FINAL DISCUSSION AND CONCLUSIONS

Using a delayed detonation model as an example, we have studied the possible influence of the initial chemical composition on the light curves and spectra of SNe Ia.

At early epochs the mean lifetime of progenitors will be smaller than at present and, hence, the mean progenitor mass is larger compared to the current epoch (see § 4). A substantially reduced C/O ratio in the inner region of the progenitor white dwarf will result if the WD originates from a star with more than  $\approx 3-4 M_\odot$  rather than  $1-2 M_\odot$  on the ZAMS. We find that a reduction of the initial C/O ratio has effects similar to a lower transition density from deflagration to detonation. In both cases, the location of the Si-rich material is shifted to smaller expansion velocity. In the case of a reduction in the C/O ratio the expansion velocity during the explosion is somewhat lower and the time is delayed until the transition density is reached. For lower transition densities, the extent of the deflagration phase is increased because a longer time is required to reach the transition density. In both cases, this allows for a longer preexpansion of the outer layers, and consequently the  $^{56}\text{Ni}$  production is reduced. The major difference between a

TABLE 4  
UNCERTAINTIES IN  $q_0$ ,  $\Omega_M$ , AND  $\Omega_\Lambda$  AS INTRODUCED BY  
COMPOSITION EFFECTS

$\Delta m$ (mag)	0.1	0.2	0.3	0.6
$q_0(z = 1)$ .....	0.1	0.2	0.3	0.6
$\Omega_M(z = 1, \Omega_\Lambda = 0)$ .....	0.2	0.4	0.6	1.2
$\Omega_M(z = 1.0, \Omega_\Lambda = 0.5, \text{flat})$ .....	0.1	0.2	0.3	0.6

reduced C/O ratio and a lower transition density is the reduced explosion energy (and expansion rate) in the former case. This causes the peak in the Si distribution to be more pronounced in velocity space, a slower rise to maximum light by about three days, an increased peak luminosity, and, consequently, a steeper decline after maximum light when the stored, thermal energy is exhausted. The use of light-curve shapes or postmaximum decline rates alone may lead to systematic errors in the estimates of the absolute brightness by several tenths of a magnitude. In principle, detailed coordinated analyses of spectra and light curves provide a way to disentangle the effects of a change in the transition density and the C/O ratio and to determine the peak brightness on a case-by-case basis. Empirically, a correlation analysis of the light-curve shape and the expansion rate provides a tool to test for the range of C/O ratios realized in nature (see § 3.2).

Changing the initial metallicity from Population I to Population II reduces the progenitor lifetime and Roche lobe radii and hence changes progenitor evolution. It also alters the isotopic composition of the outer layers. Especially important is the increase in the  $^{54}\text{Fe}$  production with metallicity. The initial WD composition has been found to have rather small effects on the overall light curves. The  $^{56}\text{Ni}$  production and hence the bolometric and monochromatic optical and IR light curves differ only by a few hundredths of a magnitude. This change is almost entirely due to the small change in the  $^{56}\text{Ni}$  production and is not due to a change in the opacities because the diffusion timescales are governed by the deeper layers where burning is complete. The time of maximum light in the Johnson filter system changes by  $\approx 1$  day as  $Z$  is varied from solar to  $\frac{1}{3}$  solar. The short-wavelength part of the spectrum at maximum light is affected by a change in  $Z$ . This provides a direct test for the initial metallicity of local SNe Ia if well-calibrated spectra are available and, thus, may give a powerful tool to unravel the nature (and lifetime) of SNe Ia progenitors. To do so, spectra around or prior to maximum light are needed because at later times the inner layers dominate the spectra where the spectrum is not sensitive to the initial metallicity (see § 3.3). Note that quantitatively the influence of  $Z$  is model dependent because it depends on the photon redistribution and optical depth at a given time, i.e., on the density and abundance structure. Even the sign of the effect of the configuration is very different from the delayed detonations. As an empirical test, a differential comparison between maximum and postmaximum spectra of different SNe Ia with similar light-curve shapes and expansion velocities provides a valuable tool to probe for  $Z$  effects (see § 3.2).

In terms of distant SNe, we may expect less metals and lower C/O ratios in the past. For redshifted supernovae, the  $Z$  effect may produce systematic changes of up to 0.2–0.3 mag in  $B-V$ ,  $V-R$ , and  $R-I$  for  $z \geq 0.2, 0.5$ , and  $0.7$ , respectively. The amplitude of the maximum change and the phase with respect to  $z$  is somewhat model dependent. In general, the C/O ratio will decrease with redshift and can be expected to become significant at redshifts  $\geq 0.7$  when the age of the universe is comparable to the lifetime of the progenitors. The systematic effects due to changing  $Z$  and C/O may be comparable in amplitude to the effects due to the deceleration of the universe. Other evolutionary effects have been qualitatively discussed in § 4 and in the Introduction. Because the properties of SNe Ia may change with

$z$ , a measurement of  $q_0$ ,  $\Omega_M$ , and  $\Lambda$  may be highly biased. Determinations of  $H_0$  will remain unaffected if they are based on a sufficiently large range of light curves (e.g.,  $B$ ,  $V$ ,  $R$ ,  $I$ ).

Finally, we also want to mention the limitations of this study, which we need to overcome in the future. First of all, only one specific set of models has been studied in detail. Although the model parameters have been chosen to allow for a representation of “typical” SNe Ia, more comprehensive studies and detailed fitting of actual observations are needed. The C/O ratio has been changed for the entire WD; however, the C/O ratio is expected to change only for the mass before binary accretion begins (e.g.,  $0.6 M_\odot \leq M_{\text{in}} \leq 1.2 M_\odot$ ). A C/O ratio of  $\approx 1$  will result from the accreted material at the surface regardless of the mass of the primary or secondary star (e.g., Nomoto et al. 1984). The final composition of the supernova ejecta which undergoes partial burning depends mainly on the density during burning. This, in turn, depends on the preexpansion during the deflagration phase because it lasts longer by an order of magnitude (i.e., about 1–2 s) compared to the detonation phase. During the deflagration phase, only the inner regions ( $\approx 0.2\text{--}0.3 M_\odot$ ) are burned. Therefore, it does not make much difference whether the C/O ratio is lower on the inside and 1/1 on the outside due to accretion or whether a globally reduced C/O ratio is considered. Nevertheless, a study of the influence of realistic structures is desired in order for the effects to be analyzed more quantitatively.

This study explored some effects that can be expected if we go back in time. Detailed comparisons with observations are ultimately needed to address the effects of composition evolution or to probe for their unimportance. To do so, well-sampled spectral and light-curve data must be available, such as those currently obtained by the Berkeley and CTIO groups. To isolate the  $Z$  effects, we would suggest that maximum spectra and postmaximum spectra be taken routinely. To acquire a full understanding of SNe Ia, detailed analyses of nearby (e.g., Virgo or closer) supernovae are needed. Such a program is justified, because there is already evidence in the current supernova sample for evolutionary effects that are not yet understood but suggest that some effects of varying composition effects are present. We might naturally expect a range in initial metallicities of SNe Ia within spiral galaxies that have ongoing star formation and between ellipticals and spirals. The same is true for the C/O ratio, which will depend on the average age of the progenitor population. Branch, Romanishin, & Baron (1996) and Hamuy et al. (1996) have shown that the mean peak brightness is dimmer in ellipticals which lack a young population. Wang, Höflich, & Wheeler (1997) have shown that the peak brightness in the outer region of spirals is similar to those found in ellipticals, but in the central region both intrinsically brighter and dimmer SNe Ia occur. Both of these effects may involve a change in the C/O ratio. SNe Ia with a low C/O ratio have a short progenitor lifetime and are predicted to be brighter. Another independent statistical test for the influence of a changing C/O ratio may be to use the spread in the velocity–light-curve shape relation. If the C/O ratio is the dominant effect to explain the spread in the properties of light curves, there should be a tight relation between light-curve shape and expansion velocity in ellipticals and a spread in spirals. Another approach to get insight into the local SNe Ia may be the use of  $\delta$  Cephei distances to evaluate the spread in the absolute brightness.

We thank the referee, D. Branch, and K. Nomoto for helpful discussions and useful comments. This research was supported in part by NSF grant AST 95-28110 and NASA grant NAG 5-2888, and a grant from the Texas Advanced Research Program, grant Ho1177/2-2 from the German

Science Foundation (DFG), grant 20-47252.96 of the Swiss Nationalfonds, and in its final stages by NSF grant PHY 94-07194 to the ITP at the University of California. The calculations were done at the High Performance Computer Facilities of the University of Texas at Austin.

## REFERENCES

- Abbot, D. C., & Lucy, L. B. 1985, *ApJ*, 288, 679  
 Arnett, W. D. 1969, *Ap&SS*, 5, 280  
 Barbon, R., Benetti, S., Cappellaro, E., Rosino, L., & Turatto, M. 1990, *A&A*, 237, 79  
 Barbon, R., Ciatti, F., & Rosino, L. 1973, *A&A*, 29, 57  
 Branch, D. 1981, *ApJ*, 248, 1076  
 Branch, D., Romanishin, W., & Baron, E. 1996, *ApJ*, 467, 73  
 Branch, D., & Tammann, G. A. 1992, *ARA&A*, 30, 359  
 Canal, R. 1994, in *Proc. Les Houches Session LIV*, ed. S. Bludman, R. Mochovitch, & J. Zinn-Justin (Paris: North-Holland), 155  
 Castor, H. U. 1974, *MNRAS*, 169, 279  
 Colella, P., & Woodward, P. R. 1984, *J. Comput. Phys.*, 54, 174  
 DiStefano, R., Nelson, L. A., Lee, W., Wood, T. H., & Rappaport, S. 1997, in *Thermonuclear Supernovae*, ed. P. Ruiz-Lapuente, R. Canal, & J. Isern (Dordrecht: Kluwer), 147  
 Filippenko, A. V., et al. 1992a, *ApJ*, 384, L15  
 ———. 1992b, *AJ*, 104, 1543  
 Goodbar, A., & Perlmutter, S. 1996, *ApJ*, 450, 14  
 Hamuy, M., Phillips, M. M., Maza, J., Suntzeff, N. B., Schommer, R. A., & Aviles, A. 1996, *AJ*, 112, 2438  
 Hansen, C. J., & Wheeler, J. C. 1969, *Ap&SS*, 3, 464  
 Harkness, R. P. 1991, in *ESO/EIPC Workshop on SN 1987A and Other Supernovae*, ed. I. J. Danziger & K. Knär (Garching: ESO), 447  
 Hernanz, M., Salaris, M., Isern, J., & Jose, J. 1997, in *Thermonuclear Supernovae*, ed. P. Ruiz-Lapuente, R. Canal, & J. Isern (Dordrecht: Kluwer), 167  
 Höflich, P. 1990, *Habilitation Thesis*, Ludwig Maximilians Univ. (MPA-90; München: MPI), 563  
 ———. 1995, *ApJ*, 443, 533  
 Höflich, P., & Khokhlov, A. 1996, *ApJ*, 457, 500  
 Höflich, P., Khokhlov, A., Nomoto, K., Thielemann, F. K., & Wheeler, J. C. 1997, in *Thermonuclear Supernovae*, ed. P. Ruiz-Lapuente, R. Canal, & J. Isern (Dordrecht: Kluwer), 659  
 Höflich, P., Müller, E., & Khokhlov, A. 1992, *A&AS*, 97, 221  
 ———. 1993, *A&A*, 268, 570  
 Hoyle, F., & Fowler, W. A. 1960, *ApJ*, 132, 565  
 Iben, I. Jr. 1997, in *Thermonuclear Supernovae*, ed. P. Ruiz-Lapuente, R. Canal, & J. Isern (Dordrecht: Kluwer), 111  
 Iben, I., Jr., & Tutukov, A. V. 1984, *ApJS*, 54, 335  
 Ivanova, I. N., Imshennik, V. S., & Chechetkin, V. M. 1974, *Ap&SS*, 31, 497  
 Karp, A. H., Lasher, G., Chan, K. L., & Salpeter, E. E. 1977, *ApJ*, 214, 161  
 Khokhlov, A. 1991, *A&A*, 245, 114  
 Khokhlov, A., Müller, E., & Höflich, P. 1993, *A&A*, 270, 223  
 Kurucz, R. P. 1993a, CD-ROM 1: Line list (CfA: Harvard University)  
 ———. 1993b, CD-ROM 23: Line list (CfA: Harvard University)  
 ———. 1996, CD-ROM: Lines and Levels for Iron Group Elements (CfA: Harvard University)  
 Leibundgut, B., Kirshner, R. P., Filippenko, A. V., Shields, J. C., Foltz, C. B., Phillips, M. M., & Sonneborn, G. 1991, *ApJ*, 371, L23  
 Leibundgut, B., et al. 1995, *ESO-Messenger*, 81, 19L  
 Livne, E., & Arnett, D. 1995, *ApJ*, 452, 62  
 Mihalas, D., Kunacz, R. B., & Hummer, D. G. 1975, *ApJ*, 202, 465  
 ———. 1976a, *ApJ*, 206, 515  
 ———. 1976b, *ApJ*, 210, 419  
 Müller, E., & Höflich, P. 1994, *A&A*, 281, 51  
 Nomoto, K. 1980, in *IAU Symp. 93, Fundamental Problems in the Theory of Stellar Evolution*, ed. D. Sugimoto, D. Q. Lamb, & D. Schramm (Dordrecht: Reidel), 295  
 ———. 1982, *ApJ*, 253, 798  
 Nomoto, K., & Sugimoto, D. 1977, *PASJ*, 29, 765  
 Nomoto, K., Sugimoto, S., & Neo, S. 1976, *Ap&SS*, 39, L37  
 Nomoto, K., Thielemann, F.-K., & Yokoi, K. 1984, *ApJ*, 286, 644  
 Nomoto, K., Yamaoka, H., Shigeyama, T., & Iwamoto, K. 1995, in *Supernovae and Supernova Remnants*, ed. R. A. McCray, Z. Wang, & Z. Li (Cambridge: Cambridge Univ. Press), 49  
 ———. 1997, in *Thermonuclear Supernovae*, ed. P. Ruiz-Lapuente, R. Canal, & J. Isern (Dordrecht: Kluwer), 349  
 Norgaard-Nielsen, H. U., Hansen, L., Henning, E. J., Salamanca, A. A., Ellis, R. S., & Warrick, J. C. 1989, *Nature*, 339, 523  
 Nugent, P., Baron, E., Hauschildt, P., & Branch, D. 1995, *ApJ*, 441, L33  
 Nugent, P., Baron, E., Branch, D., Fisher, A., & Hauschildt, P. 1997, *ApJ*, 485, 812  
 Olson, G. L., Auer, L. H., & Buchler, J. R. 1986, *J. Quant. Spectrosc. Radiat. Transfer*, 35, 431  
 Paczyński, B. 1985, in *Cataclysmic Variables and Low-Mass X-Ray Binaries*, ed. D. Q. Lamb & J. Patterson (Dordrecht: Reidel), 1  
 Pennypacker, C., et al. 1991, *IAU Circ.*, 5207  
 Perlmutter, S., et al. 1997, *ApJ*, 483, 565  
 Phillips, M. M., et al. 1987, *PASP*, 90, 592  
 Pskovskii, Yu. P. 1970, *AZh*, 47, 994  
 ———. 1977, *Soviet Astron.*, 21, 675  
 Rappaport, S., Chiang, E., Kallman, T., & Malina, R. 1994a, *ApJ*, 431, 237  
 Rappaport, S., DiStefano, R., & Smith, J. 1994b, *ApJ*, 426, 692  
 Riess, A. G., Press, W. H., & Kirshner, R. P. 1995, *ApJ*, 438, L17  
 Samland, M., Hensler, G., & Theis, C. 1997, *ApJ*, 476, 544  
 Sandage, A., & Tammann, G. A. 1993, *ApJ*, 415, 1  
 Schaller, G., Schaerer, D., Meynet, G., & Maeder, A. 1992, *A&AS*, 96, 269  
 Schmidt, B. P., et al. 1996, *BAAS*, 189, 1089  
 Sobolev, V. V. 1957, *Soviet Astron.*, 1, 297  
 Thielemann, F.-K., Nomoto, K., & Hashimoto, M. 1996, *ApJ*, 460, 408  
 Thielemann, F. K., Nomoto, K., Iwamoto, K., Brachwit, F. 1997, in *Thermonuclear Supernovae*, ed. P. Ruiz-Lapuente, R. Canal, & J. Isern (Dordrecht: Kluwer), 485  
 Thielemann, F.-K., Nomoto, K., & Yokoi, K. 1986, *A&A*, 158, 17  
 van den Heuvel, E. P. J., Bhattacharya, D., Nomoto, K., & Rappaport, S. 1992, *A&A*, 262, 97  
 Wang, L., Höflich, P., & Wheeler, J. C. 1997, *ApJ*, 483, 29  
 Webbink, R. F. 1984, *ApJ*, 277, 355  
 Wheeler, J. C., & Harkness, R. P. 1990, *Rep. Prog. Phys.*, 53, 1467  
 Wheeler, J. C., Harkness, R. P., Khokhlov, A., & Höflich, P. 1995, *Phys. Rep.*, 256, 211  
 Woosley, S. E., & Weaver, T. A. 1986, *ARA&A*, 24, 205  
 ———. 1994a, *ApJ*, 423, 371  
 ———. 1994b, in *Proc. Les Houches Session LIV*, ed. S. Bludman, R. Mochovitch, & J. Zinn-Justin (Paris: North-Holland), 63  
 Woosley, S. E., Weaver, T. A., & Taam, R. E. 1980, in *Type I Supernovae*, ed. J. C. Wheeler (Austin: Univ. Texas), 96  
 Yamaoka, H., Nomoto, K., Shigeyama, T., & Thielemann, F. 1992, *ApJ*, 393, 55